A procedure for quantitative characterization of superparamagnetic minerals in environmental magnetism

Arua S. Leite, Carlos A. Mendonça, Pedro L. A. Moraes, Andrea T. Ustra

HAL Id: insu-03661387

https://insu.hal.science/insu-03661387

Submitted on 6 May 2022

Geophysical Journal International

A procedure for quantitative characterization of superparamagnetic minerals in environmental magnetism

Arua S. Leite,[1,2] Carlos A. Mendonça,[1] Pedro L.A. Moraes[1] and Andrea T. Ustra[1]

[1]*Department of Geophysics, University of Sao Paulo, Sao Paulo, Brazil. E-mail: arualeite@gmail.com*
[2]*Geosciences Environnement Toulouse, University Paul Sabatier, Toulouse, France.*

SUMMARY

Ultrafine grains of magnetic minerals provide reliable recordings of both naturally occurring and anthropogenically generated particulate matter in polluted air; magnetic data can be used to understand biogenic iron-cycling in anaerobic environments, as well as pedogenesis and palaeoclimate studies of loess soils. The ultrafine fraction is produced under specific conditions and can be easily recognized by its superparamagnetic (SP) behaviour. Many proxies have been proposed to account for the SP contribution by measuring its susceptibility dependency with frequency (frequency effect) or the magnetization loss after removing an external inducing field. Here we introduce the Superparamagnetic Concentration and Dipole Moment (SPCDM) procedure for quantitative interpretation of SP magnetization. This procedure is well suited to SP carriers with a fast magnetization decay (<1 s), as would be expected for magnetic minerals with a grain size distribution lying below the blocking volume for stable, single-domain (SD) magnetization. SPCDM requires a dedicated experimental procedure to isolate the SP response from the paramagnetic and remnant effects, as observed in samples with mixed contributions. The proposed technique was tested using synthetic, nanoparticles of magnetite and then to characterize the magnetic properties of air particulate matter (PM) sampled at Jânio Quadros tunnel in São Paulo, Brazil. For nano-sized magnetite, SPCDM estimates for dipole moment are invariable with mass concentration and consistent with the published results; estimates for particle concentration are strongly correlated with true mass concentration ($R^2 = 0.96$). For air PM, SPCDM estimates a particle size with a diameter of 7.7 ± 0.1 nm, a kind of ultrafine magnetic material not previously recognized in air pollutants.

Key words: Magnetic properties; Environmental magnetism; Rock and mineral magnetism; Inverse theory.

1 INTRODUCTION

Fine and ultrafine agnetic minerals ($<\mu$m) found in rock, soils and air particulate matter are indicators of natural and anthropogenic processes affecting the iron cycling in shallow and deeper levels of the Earth's crust. Such magnetic mineral fractions are important for two reasons. First, few geochemical and biogeochemical processes are able to produce or modify such small grains in soils and rocks (Taylor *et al.* 1987; Maher & Taylor 1988; Maxbauer *et al.* 2016) and secondly, their characteristic superparamagnetic (SP) response can be recognized with common soil and rock magnetism procedures (Moskowitz *et al.* 1989,1993; Tadurno 1995).

In general, the SP content can be recognized in the frequency domain by the susceptibility 'frequency effect' (Dearing *et al.* 1996), from measurements achieved in at least two frequencies (470 and 4700 Hz, for Bartington Instruments Ltd). The susceptibility variation with frequency is minor (to null) in the absence of SP minerals

and so no frequency effect is produced in such cases. The SP behaviour can also be identified in time domain measurements by measuring the magnetization decay ('viscous decay') after turning off an inducing magnetic field applied to the sample (Worm 1999; Wang *et al.* 2010). Measurements in the time domain require an adequate time window and resolution tag to capture the magnetization decay waveform. A time window of 100 s is usually employed (Wang *et al.* 2010) and the decay rate is evaluated by the difference between magnetization at $t = 0$ and 100 s after the external field removal, normalized by the initial ($t = 0$) magnetization. This quantitative proxy for recognizing SP contents was introduced by Worm (1999) and improved by Machac *et al.* (2007) by introducing a set of intervals and field intensities. A close association between time and frequency domain percentage parameters was observed (Machac *et al.* 2007) despite the fact that both approaches only provide semiquantitative estimates for mass or volume concentration of SP minerals. It can be explained because both time and fre-

quency percentage parameters (frequency effect and magnetization decay) result from mixed contributions of mineral type, grain size and concentrations, therefore they are not simple indicators of concentration itself. These percentage proxies are partly conditioned by acquisition parameters, making the comparison of different datasets no simple matter. Magnetization decay, evaluated in time windows of 15 s (Worm 1999) and 60 s (Machac *et al.* 2007), for example, are not necessarily correlated because decay rates are sensitive to minor variations in grain size. Wang *et al.* (2010) improved time-domain studies by using a J-meter coercivity spectrometer (Jasonov *et al.* 1998; Wang *et al.* 2010) and measuring the magnetization immediately after the external field removal. There is also an extensive literature on using relaxation-based methods based on Néel theory for characterization of nanoparticle populations, under conditions for which the net magnetization is time-dependent over the measurement interval (e.g. Worm & Jackson 1999; Shcherbakov & Fabian 2005; Jackson *et al.* 2006; Egli 2009; Kodama 2013).

Previous works proposed different approaches to deal with magnetic grains exhibiting SP behaviour. Through the fitting of the Langevin function for a magnetization curve, they allow reconstructing the magnetic moment (or volume) distribution in synthetic samples. Berkov *et al.* (2000), using diluted ferrofluid samples propose fitting sums (or weighted integrals) through the singular value decomposition (SVD) technique and linear constraints to recover the distribution of magnetic moments. Woodward *et al.* (2007) compare measuring methods for the particle-size distribution of magnetic nanoparticles (transmission electron microscopy; Langevin fitting and small-angle neutron scattering). The Langevin fitting was accomplished by least-squares routines taking *a priori* assumptions about the distribution form. As developed in SPCDM, the Langevin fitting is applied after correcting IRM contributions, thus allowing the study of mixed samples as found in geological and environmental investigations. The SPCDM application to pure SP samples have much in common with previous work with synthetic materials.

A better characterization of the SP fraction allows the investigation of a diversity of problems in environmental magnetism. SP minerals can be formed as a consequence of variable redox conditions during wet and dry cycles (Maxbauer *et al.* 2016) and these result in indicators that allow recovery environmental and depositional conditions in complex sedimentary basins, as well as helping us to understand records of climate change in palaeosols and loess deposits (Maher & Thompson 1991; Porter 2001). SP particles are also generated during dissimilatory iron reduction (DIR) in anoxic conditions, where oxidation of organic matter becomes coupled with microbial reduction of Fe(III) oxides, with extracellular precipitation of ultrafine magnetite (Moskowitz *et al.* 1989; Jimenez-Lopez *et al.* 2010; Li *et al.* 2013).

In addition to natural processes, ultrafine magnetic minerals are also generated by industrial and transportation systems (fossil fuel combustion, disk-breaks, pavement abrasion, etc.) and these allow the application of magnetic measurements in pollutant provenance studies and air quality in urban areas (Sagnotti & Winkler 2012). Magnetic fractions in air particulate matter also serve as tracers for associated pollutants with ultrafine grain size (Sagnotti *et al.* 2006), for which safe exposure limits are not well established (Donaldson 2003; Bealey *et al.* 2007). Air particulate matter (PM) with aerodynamic dimensions below 0.1 μm ($PM_{0.10}$) has been a topic of concern in health sciences because of their capacity to reach deeper parts of the respiratory system, thereby enhancing the deleterious effects of associated hazardous substances (Morris *et al.* 1995; Pope *et al.* 2002; Calderón-Garcidueñas *et al.* 2008).

Despite their importance in environmental magnetism, the common techniques used to characterize SP fractions are not effective in answering key questions (Evans & Heller 2003) about quantitative estimates for mass/volume concentration, grain size distribution and mineral types, among others. Most techniques based on data acquisition proxies (frequency effect or decay rate, for example) can be regarded as not being effective in addressing such questions. We develop a quantitative procedure—SPCDM (Superparamagnetic Concentration and Dipole Moment)—to determine the concentration and the dipole moment of the magnetic carriers with SP behaviour. When the magnetic mineral is known (or assumed *a priori*), quantitative estimates of mean grain size (though not of the size distribution) and particle concentration are obtained. An adequate database and processing scheme is required in order to isolate the SP response before determining the unknown parameters in the Neel's model (sample specific saturation magnetization and grain dipole moment) with non-linear data inversion procedures. Particle concentration is then estimated from a basic, constitutive relationship relating the model parameters obtained from data inversion. SPCDM is validated by a control experiment, comprising samples with different concentrations of nano-sized synthetic magnetite within a narrow size distribution and then applied to analyse air particulate matter from air-quality monitoring stations installed in the Jânio Quadros tunnel in São Paulo, Brazil.

2 THEORY

2.1 Model construction

Single-domain, ferromagnetic minerals exhibit an SP response when reduced to grain sizes down to a critical blocking volume that is not able to sustain permanent magnetization at room temperature. Below this blocking volume, the orientation of the particles magnetic moments is disturbed by thermal fluctuations resulting in null bulk magnetization. When exposed to an external static field, the dipole moments are aligned with the inducing field sustaining a net magnetization as long as the inducing field is kept active, otherwise it vanishes. For an assemblage of uniform grains, this unstable magnetization decays according to the formula (Evans *et al.* 2003)

$$M(t) = M_0\, e^{\frac{-t}{\tau}}, \tag{1}$$

starting from magnetization M_0 when $t = 0$ (when the inducing field is turned off). Magnetization $M(t)$ decays according to a characteristic relaxation time τ given by Néel (1955) and

$$\tau = \tau_0\, e^{-\frac{E_M}{E_T}}, \tag{2}$$

where τ_0 is a time-factor varying from 10^{-12} to 10^{-8} s (Dormann *et al.* 1996; Worm 1998) and accounts for a characteristic time-lag between successive random thermal fluctuations (Berndt *et al.* 2015). $E_M = Kv$ represents the magnetostatic energy barrier required to switch the magnetic dipole direction, K [Jm^{-3}] is the grain coefficient of anisotropy and v [m^3] is its volume. Thermal energy ($E_T = k_B T$) counteracts magnetic ordering by randomly flipping the grain dipole directions; $k_B = 1,38 \times 10^{-23}$ [JK^{-1}] is the Boltzmann constant and T [K] is the temperature. The coefficient of anisotropy is given by the equation $K = \mu_0 H_k \sigma_S / 2$, where H_k [Am^{-1}] is the microscopic coercivity of the grain, such that $H_k = 2.09 H_c$ (Stoner & Wohlfarth 1948). Term H_c is the sample macroscopic coercivity and σ_S is the saturation magnetization of the mineral species.
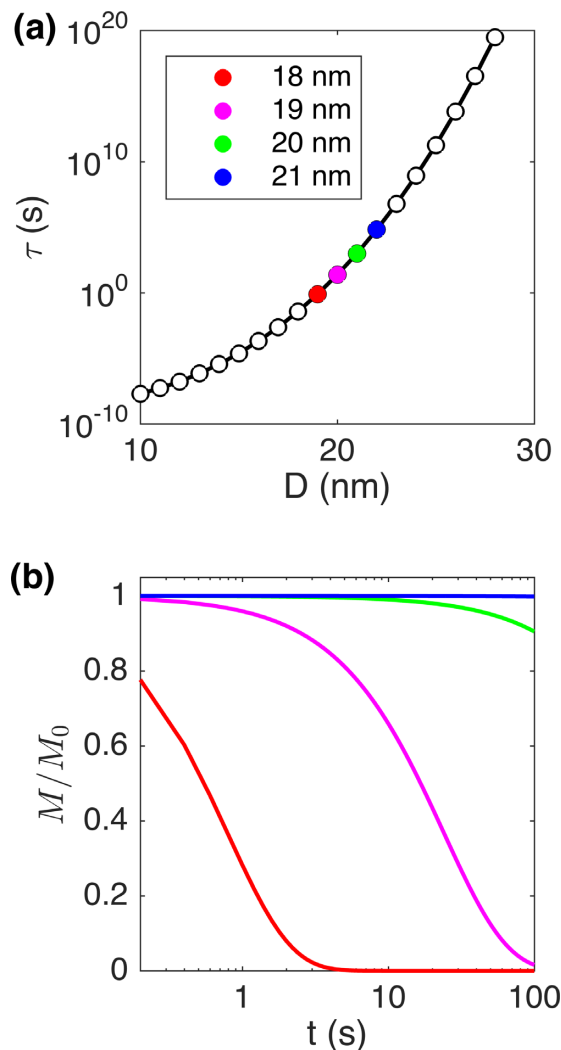
Figure 1. (a) Variations of relaxation time with diameter of spherical magnetite-like minerals and (b) corresponding magnetization decay normalized by initial magnetization M_0. Blocking volume with stable magnetization (blue), thermally active particles with viscous (green and magenta) and fast (red) magnetic relaxation as expected in 100 s window.

For measurements at a constant temperature, the relaxation time τ is conditioned by grain size v and magnetic anisotropy K; both parameters express physical properties of the magnetic carriers. Fig. 1 illustrates the wide variation of relaxation times from minor changes in diameter that would be expected from spherical particles of magnetite (mineral specific saturation magnetization $\sigma_S =$ 480 kAm^{-1}, $K = 2.31 \times 10^4$ Jm^{-3}). The magnetization decay can be relatively fast ($\tau = 1.98 \times 10^{-8}$ s) for grains with diameters of 10 nm, in the 100 s time window for grains with diameters of 20 nm, and stable (9.4×10^{11} yr) for grains with diameters of about 28 nm. Experimental data shows that blocking volume for magnetite has a diameter between 25 and 30 nm (Dunlop & Özdemir 2001) and approximately 17 nm for hematite (Jiang *et al.* 2014).

Fig. 1(b) is effective in showing how minor grain size variations may lead to substantial changes in the magnetization decay rate. This change is particularly sensitive in particles below a few nanometres in diameter with respect to a reference grain diameter for a blocking volume, sustaining stable magnetization in SD grains. It can be seen that a very narrow grain size distribution is associated with magnetization decay waveforms that are able to be captured in

the 100s time-window, as have been observed in SP studies (e.g. Worm 1999; Wang *et al.* 2010). For broader ranges of grain sizes below this limit fast decay rates (in milliseconds or microseconds) are expected. This faster decay behaviour may be within the time resolution interval of common equipment or in the range of transient coil induction fields, preventing further analysis based on modelling the magnetization waveform decay. Nevertheless, a 'slow' decay rate (e.g. one captured in the 100 s time-windows) is indicative of a coarser SP fraction nearing the characteristic blocking volume for SD grains.

For pure (non-mixed) ultrafine grains, the transient magnetization vanishes to zero within intervals of microseconds, henceforth termed 'fast SP decay'. This type of fast decay can be associated with particles of a grain size well below the critical volume for stable magnetization. For mixed SP-SD or SP-MD mineral fractions, the SP magnetization appears superimposed to stable magnetization. Fig. 2 illustrates cases of fast decay rates observed for pure (Figs 2a and b) and mixed (Figs 2c and d) SP samples. Fast decay rates are observed in samples with nanoparticles of magnetite dispersed in paraffin (see Section 3) in a similar way to rates seen in air PM collected in the Jânio Quadros tunnel in São Paulo (Section 4). The air PM sample also exhibits IRM acquisition, according to the intensity of the inducing field and, as such, indicates a mixed contribution of magnetic carrier with grain sizes in the SP and SD-MD fractions.

Slower magnetization decay is observed in the sediments from the Jaraguá Cavern in São Paulo, as magnified in Fig. 3 for samples exposed to an external field of 500 mT. Fig. 3 illustrates that fast decay SP relaxation does occur in samples from air PM and are, therefore, indicative of ultrafine grain size distributions that have not been well accounted for in previous studies.

For pure (non-mixed) ultrafine grains (e.g. Figs 2b and c), the transient magnetization vanishes to zero in microseconds; and is associated with particles of grain sizes well below the critical volume for stable magnetization. In exploration geophysics terms, this type of magnetization is known as 'induced magnetization' (Telford *et al.* 1990) and it appears superposed to stable magnetization in mixed SP-SD or SP-MD mineral fractions.

The SP contribution under the H_0 [Am^{-1}] external field is given by eq. (3) (Dunlop & Özdemir 2001)

$$M(H_0, T) = M_S L(\alpha),\qquad(3)$$

where

$$\alpha = \frac{\mu_0 v \sigma_S H_0}{k_B T}\qquad(4)$$

and $L(\alpha)$ is the Langevin function:

$$L(\alpha) \equiv coth\left(\frac{\mu_0 v \sigma_S H_0}{k_B T}\right) - \frac{k_B T}{\mu_0 v \sigma_S H_0}.\qquad(5)$$

In eq. (3), M_s is the sample specific saturation magnetization and $\mu_0 = 4\pi \times 10^{-7}$ [Hm^{-1}] is the free space permeability. For hematite, σ_S is approximately 0.5 per cent that of magnetite (Dunlop & Özdemir 2001). The grain dipole moment is $\mu = v\sigma_S$ [Am^2] and the sample saturation magnetization is $M_S = n\mu$ [Am^{-1}]. Term n [m^{-3}] is the concentration (number of particles per volume) of the magnetic carriers. For a sample with density ρ [kgm^{-3}], the mass-concentration of the magnetic carriers is obtained by n/ρ. The concentration of SP carriers (n) does not necessarily express the concentration of particulate matter, except under a very particular condition in which single magnetic particles are attached to single grains in the soil or particulate matter.
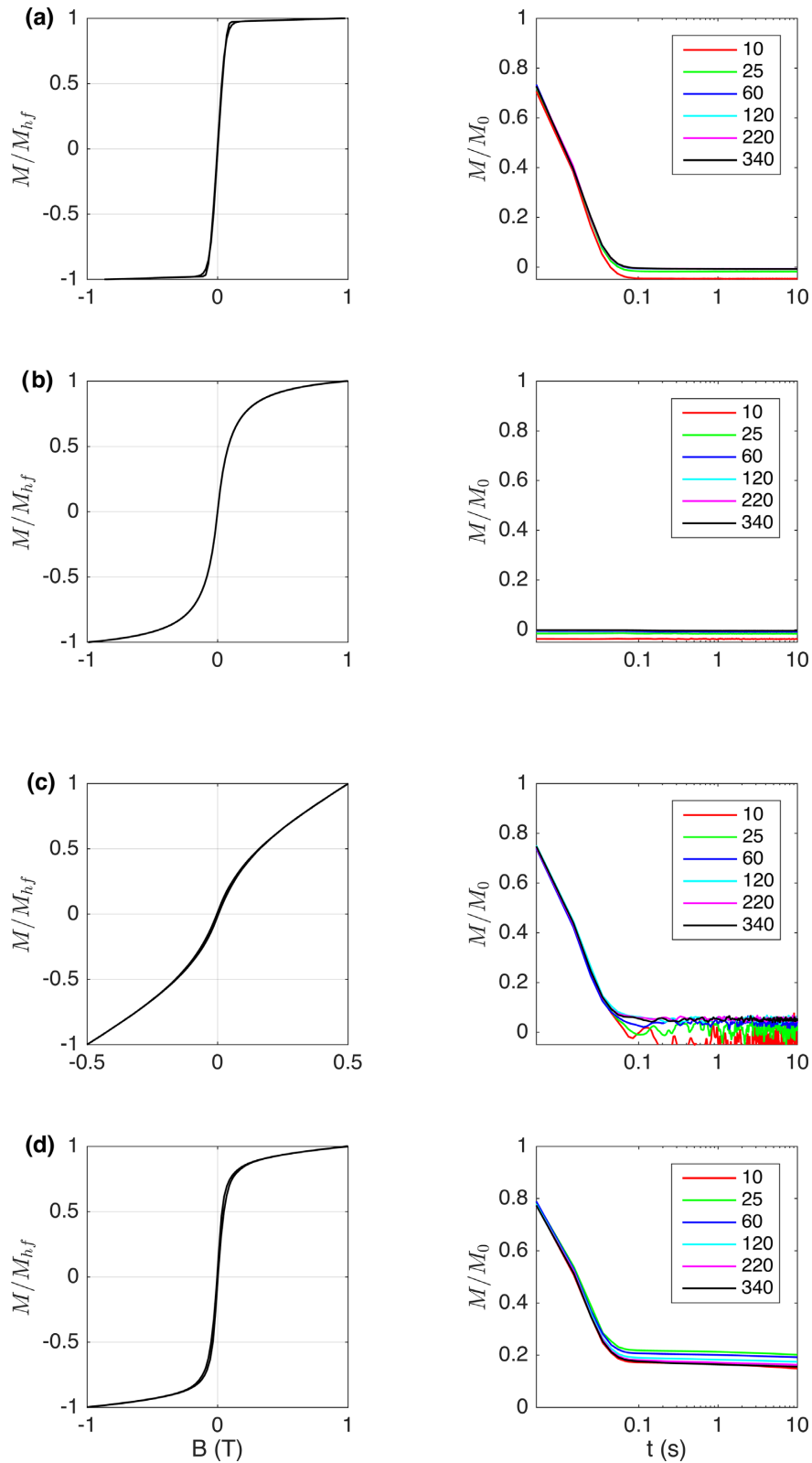
Figure 2. Hysteresis curves (left) normalize by high-field magnetization M_{hf} (magnetization expressed in fields of 1 and 0.5 T) and magnetization decay curves (right) normalized by in field magnetization M_0 (magnetization measured during external fields applications); (a) calibrator 2853 YIG Sphere with pure SP behaviour; (b) nanoparticles of synthetic magnetite with 8 nm diameter; (c) air particulate matter collected in Jânio Quadros tunnel, São Paulo; (d) sediments from Jaraguá Cave, São Paulo with subtle magnetic decay in 100s window. Pure SP response is observed in sample (a),(b); combined SP and IRM responses observed in samples c and d. Zero-crossing in hysteresis curves for sample b is consistent with pure SP composition; low coercivity in samples (c) and (d) is indicative of magnetite-like minerals comprising a coarser fraction with IRM response. The decay curves for in fields of 10, 25, 60, 120, 220 and 340 mT. SPCDM data have 17 in field inductions, for illustration only 6 are presented.
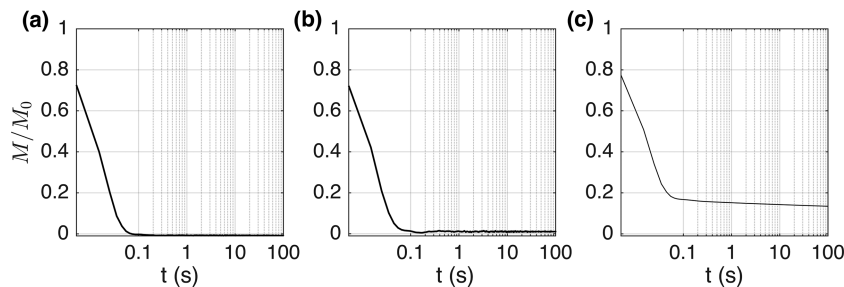
Figure 3. Magnetization relaxation after applying a 500 mT normalized by in field magnetization M_0; (a) nanoparticle of synthetic magnetite with fast relaxation; (b) air particulate matter with same behaviour and (c) sediments from Jaraguá Cave with slower magnetization decay, suggestive of coarser SP minerals.

Under isothermal conditions, the SP magnetization dependence on the external field $B = \mu_0 H_0$ is written as $M(B) \equiv M(B, T)$, such that

$$M(B) = M_S L\left(\frac{\mu B}{k_B T}\right). \quad (6)$$

From estimates of grain dipole moment μ, and by assuming that the magnetization saturation σ_S is known, particle volume v can be determined by constitutive relationship $\mu = v\sigma_S$. By assuming particles with spherical shape, diameter estimates can be achieved.

2.2 Inverse problem formulation

According to eq. (6), SP magnetization is described in terms of two unknown parameters: M_S and μ. These parameters can be determined under an inverse problem formulation by considering a data set with N measurements of magnetization, $M_i^o \equiv M(B_i)$, when exposed to external fields B_i, $i = 1 : N$. The unknown parameters can be determined by minimizing a least-squares functional $Q(M_S, \mu)$ such that

$$Q(M_S, \mu) = \sum_{i=1}^{N}\left[M_i^o - M^c(B_i, M_S, \mu)\right]^2, \quad (7)$$

where the superscript o and c stand for 'observed' and 'calculated' magnetization values. According to inverse problem terminology (Aster *et al.* 2011), the minimization of functional in eq. (7) configures a non-linear problem because one of the unknown parameters (μ) appears as an argument of a non-linear function. The determination of the unknown parameters then requires a non-linear optimization procedure, usually converging with iterative steps, starting from an initial solution (or set of solutions) until reaching a data fitting criterion $Q(M_S, \mu) \leq \varepsilon$ or stop condition. Parameter ε establishes the acceptability condition for data fitting, according to experimental error in the data.

The set of solutions minimizing the functional Q can be accessed by mapping this function within a parameter space window and provide a visual representation of solutions satisfying $Q \leq \epsilon$ as well as possible alternative solutions (if they exist). This mapping is done by evaluating functional $Q(M_S, \mu)$ for a mesh of values (M_S, μ) in the parameter window $M_{S,l} \leq M_S \leq M_{S,u}$ and $\mu_l \leq \mu \leq \mu_u$, as defined by the lower (l) and upper (u) limits for the searched parameters. The solutions domain in this mapping appear below a contour level ('water level') which is established by threshold ε. Domain projection towards the coordinate axes M_S and μ with the unknown parameters provides a visual representation for the uncertainty of the parameters in this modelled solution. Uncertainty analysis can also be carried out by finding multiple solutions or

computing the parameters covariance for single solutions (Aster *et al.* 2011).

2.3 Experimental aspects

An experimental procedure was devised to isolate the SP response in mixed carrier samples. The proposed procedure is well suited for samples with fast SP decay, as expected for ultrafine particles discussed in Section 2.2. For mixed SP-SD (or SP-MD) samples, the magnetization decays from magnetization $M_0 \equiv M_0(B_i)$, achieved under field B_i, at $t = 0$ s to isothermal, remnant magnetization $M_q \equiv M_q(B_i)$. Once corrected for paramagnetic effects, the difference $M_0 - M_q$ can be regarded as isolating the SP response and, as such, well suited to be modelled according to eq. (6). For pure SP response, the magnetization decay rate is represented as $M(t)/M_0 = \exp(-t/\tau)$ (eq. 1) and for mixed SP-IRM contributions, by the expression $[M(t) - M_q]/[M_0 - M_q] = \exp(-t/\tau)$. The MicroMag3900-VSM measures the sample dipole moment S_D [Am^2], and not the magnetization M [Am^{-1}]. The relationship between the two is $S_D = MV$ (Evans & Heller 2003), where V is the volume [m^3] of the sample. Thus, the sample dipole saturation S_{DS} [Am^2] is given by $S_{DS} = M_S V$.

The procedure devised to provide a database for the proposed technique followed the following steps. Initially, the sample was AF-demagnetized (120 Hz, from 1T to zero in 2 per cent increments) and then subjected to external fields B_i of 5, 10, 15, 20, 25, 30, 40, 60, 80, 100, 120, 140, 180, 220, 260, 300 and 340 mT, where $i = 1 : 17$ during 10 s intervals. Longer exposures of 20 and 40 s were tested but this gave equivalent results. The magnetization M_0 is measured when the external field is on, setting $t = 0$ s when this field is turned off. Magnetization decay $M(t)$ is then recorded and averaged between 2 and 4 s to obtain equilibrium magnetization M_q. In general, a flat baseline for magnetization was achieved as fast as 10 to 20 ms after the external field was turned off, within coil inductive effects. For the tested samples, the averaging window from 2 to 4 s was unaffected by such effects, thus giving a baseline equilibrium for magnetization M_q. The differences $M_i^o \equiv M_0(B_i) - M_q(B_i)$ were then computed for external fields B_i, to isolate the sample SP response. Magnetization decay of SD and MD grains occurs at time lengths above 100 s (Fabian 2003; Williams & Muxworthy 2006) and tends to be cancelled when computing $M_0 - M_q$. This is strictly true when viscous decay is not observed in the time-window in which M_q is averaged and this difference computed. Errors were estimated by repeating the acquisition procedure for the calibrator sample (2853 YIG Sphere) 15 times. The percentage error was then evaluated and applied to measurements with tested samples. Paramagnetic

correction was carried out by the approach to saturation method, developed by Jackson & Sølheid (2010). This correction was implemented through the scripts introduced by Paterson *et al.* (2018), using the estimated paramagnetic susceptibility χ and calculated it for each field Bi as χB_i to remove the paramagnetic response from M_i^0 estimates.

2.4 Computational aspects

The SPCDM codes were implemented in two main steps. Data files from MicroMag3900 were processed according to the procedures described in Section 2.3, to isolate the SP response. An inverse procedure (as described in Section 2.2) was then applied to minimize $Q(S_{DS}, \mu)$. The minimization of this function was achieved with the FMINCON function of the Matlab Optimization Toolbox, based on the interior point algorithm of Byrd *et al.* (2000). As an iterative procedure, FMINCON requires an initial solution, which, in SPCDM, was chosen randomly within a feasibility interval, guaranteeing the parameters positivity. The optimization procedure was applied 10 times for each data set, starting from random initial solutions in order to probe alternative solutions and uncertainty. The set of resulting solutions were then used to evaluate mean $\hat{S}_{DS}$ and $\hat{\mu}$ model parameters and their respective standard deviations. These mean-solution values were used to check data fitting and evaluate SP concentration according to $\hat{n} = \hat{S}_{DS}/\hat{\mu}$. It is worth noting that SPCDM estimates for concentration did not necessarily give the particulate matter concentration, except under very particular situations in which single magnetic carriers were attached to single particles in the particulate matter. A factor expressing how many magnetic particles are attached to air PM grains is required to better evaluate air PM concentration from SPCDM estimates.

2.5 Quantifying SP contribution in total magnetization

In order to evaluate the contribution of the SP fraction in total magnetization we apply the parameter

$$\%SP = \left(\frac{M_{SP,\,1T}}{M_{H,\,1T}}\right) * 100, \tag{8}$$

which relates SP magnetization $M_{SP,1T} \equiv M(\hat{\mu}, \hat{S}_{DS}, B_{1T})$ calculated from eq. (6) and total magnetization $M_{H,1T}$ as measured in the hysteresis curve. This parameter can be evaluated under other external field intensities but the value of 1T is advised to take into account contributions from high coercivity (hematite-like) minerals, as well as to saturate SP and IRM magnetization. Parameter %SP is not related to data acquisition parameters (frequency range, time intervals or field intensity), especially considering that it varies little, when evaluating for external fields high enough to saturate both SP and IRM magnetizations.

3 SPCDM APPLICATIONS

3.1 Nanoparticles of synthetic magnetite

The first set of samples to test the SPMDM procedure comprised nanoparticles of synthetic magnetite with a mean diameter of 8 nm. These nanoparticles were synthesized according to a thermo-decomposition process reducing a Fe(III) solution under boiling temperature (>200 °C) in the presence of stabilizing agents, controlling the growth of the magnetite precipitates. A common aliquot

of nanoparticles was used to prepare 0.2, 1.0, 1.9, 3.2, 4.4 and 5.0 per cent of mass concentration by mixing with paraffin. As illustrated in Fig. 2(b) for a 5 per cent concentration sample, the nanoparticles have a pure SP behaviour at room temperature, as expressed by null coercivity in the hysteresis curve and fast magnetization decay. Its fast SP decay rate is compatible with the analysis based on Fig. 1. Fig. 4 shows SPCDM results with inverted model parameters and respective data fitting for a sample with a concentration of 5 per cent. Fig. 4(b) shows the objective function mapping, centred at the solution model obtained from data inversion. The narrow domain of alternative solutions and the absence of alternative local minima, guarantees the uniqueness for the inverted parameters.

Table 1 presents SPCDM results for the samples tested, with nanoparticles of magnetite at different concentrations. For each sample, the inversion procedure was repeated 10 times, starting with a randomly chosen solution to determine the spreading range for the inverted solutions.

The results in Table 1 show that, independent of sample concentration, the grain dipole moment estimated for the magnetic carrier is practically the same. This gives consistency to SPCDM results regarding that all tested samples were prepared with particles sharing common specifications, in terms of grain size and composition. As suggested by this test, the SPCDM estimates for grain dipole moment are not distorted by particle concentration, thus recovering an important property of magnetic carriers. The mean grain dipole moment of $1.07 \times 10^{-19} \pm 0.01$ Am^2 was estimated for the grains, which is in agreement with previous estimates of (0.85×10^{-19} Am^2) for grains of magnetite with 8 nm diameter, as presented by Ge *et al.* (2007).

Fig. 5 shows the SPCDM estimate for the mean grain dipole moment for nanoparticles of magnetite, in addition to published results for magnetite with different grain sizes (Goya *et al.* 2003; Ge *et al.* 2007; Sievers *et al.* 2012). Also in Fig. 5, is a reference to curve for model $\mu = v\sigma_S$, assuming $\sigma_S = 480$ kAm^{-1} (saturation magnetization for magnetite) and spherical particles when evaluating volume v. Despite a paucity of dipole moment data for nano-sized magnetite, one can observe a good agreement between data and model predictions, suggesting that dipole moment estimates can be used for preliminary inferences about the particle diameter of magnetite-like minerals with fast SP decay. For the nanoparticles of magnetite tested here, a mean diameter of 7.5 ± 0.2 nm was estimated, in agreement with diameter determination from the TEM image (Fig. 5), which points to real diameters of 8.0 ± 0.7 nm. It should be stressed that this is a preliminary inference but, in principle, it promises to be useful in environmental studies where pollutant provenance for distinctive grain sizes can be indicative of specific sources.

SPCDM estimates for mass-concentration (parameter n_m) from Table 1 were plotted in Fig. 6 with respect to true mass concentration, producing a clear linear dependence ($R^2 = 0.96$). This result validates the SPCDM procedure as a quantitative technique to determine concentrations of magnetic fractions in fine and ultrafine grain sizes.

Estimates for parameter %SP (Table 1), representing the contribution of SP magnetization in total magnetization under the 1 T field, reach 98.5 per cent. This result confirms that magnetization of nano-sized magnetite keeps no IRM, holding magnetization only (∼100 per cent) from the SP contribution. The ∼1.5 per cent difference may be due to accuracy limits in retrieving model parameters from the inversion of noisy data and experimental errors or measuring total field magnetization.
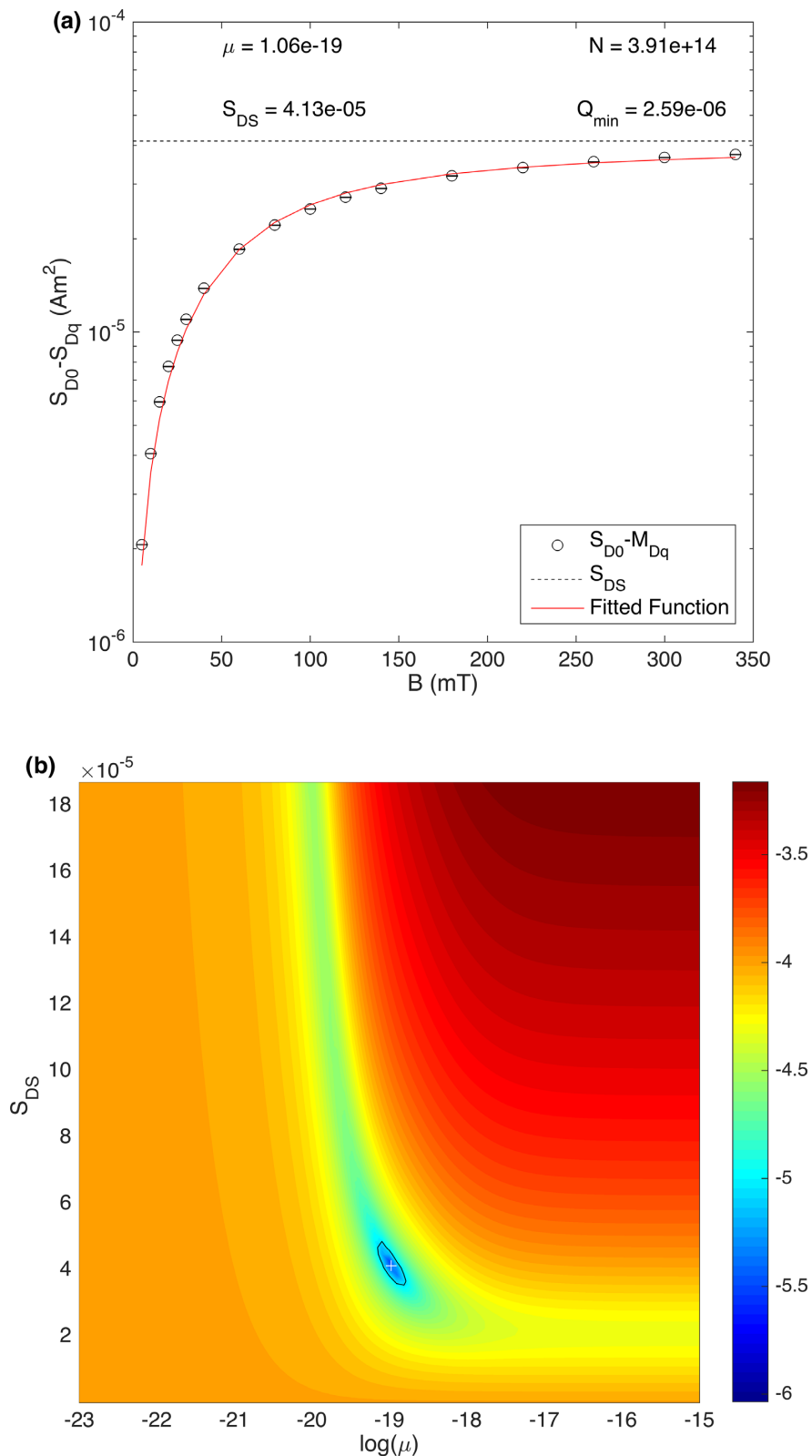
Figure 4. Inversion products of the SPCDM procedure; (a) data fitting and estimated parameters grain dipole moment μ [Am^2]; sample dipole saturation S_{DS} [Am^2] and number of magnetic carriers N. Measured data (black circles) and fitting curve (red) from the inverted model parameters. (b) Objective function with inverted model solution (white cross). For the sake of graphical representation the value of $10 \, \varepsilon$ is contoured (black) for a threshold data fitting ε equal to 5.0E-8, with stop criterion $Q_{\min} < \varepsilon$.

Table 1. SPCDM results for synthetic samples of nanoparticles of magnetite with variable mass-concentration (per cent) in paraffin; μ and S_{DS} are the grain dipole moment and sample dipole saturation, respectively; n_m is mass-concentration of magnetic carriers (number of magnetic carriers per sample mass); %SP is the contribution of SP magnetization in total magnetization under external field of 1 T. $S_{DS} = M_S\,V$ where M_S is sample saturation magnetization and V is sample volume.
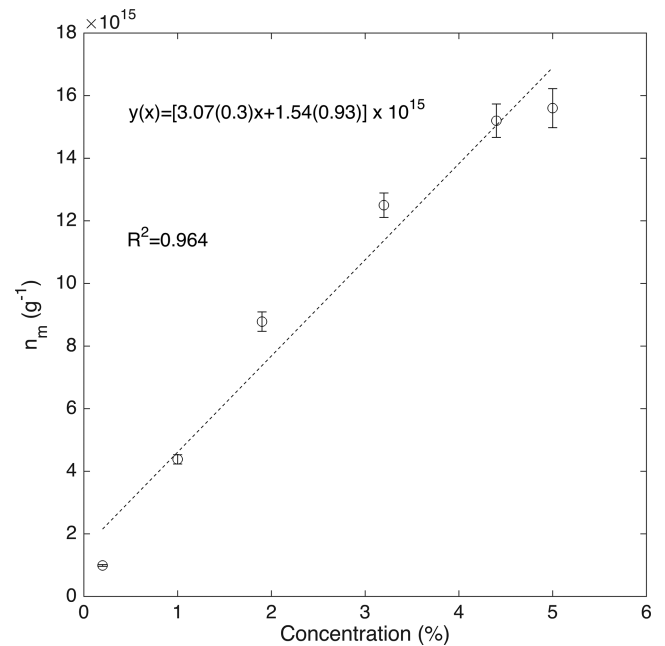
Conc. (%)	$\mu\,(10^{-19}\,\mathrm{Am^2})$	$S_{\mathrm{DS}}\,(10^{-5}\,\mathrm{Am^2})$	$n_{\mathrm{m}}\,(10^{15}\,\mathrm{g^{-1}})$	%SP
0.2	1.07 ± 0.01	0.39 ± 0.00	0.99 ± 0.03	98.5
1.0	1.06 ± 0.00	1.39 ± 0.01	4.38 ± 0.15	98.7
1.9	1.06 ± 0.01	2.99 ± 0.01	8.78 ± 0.31	98.9
3.2	1.07 ± 0.01	4.30 ± 0.00	12.50 ± 0.40	98.6
4.4	1.08 ± 0.01	6.71 ± 0.02	15.20 ± 0.50	98.6
5.0	1.06 ± 0.00	4.13 ± 0.00	15.60 ± 0.60	98.9
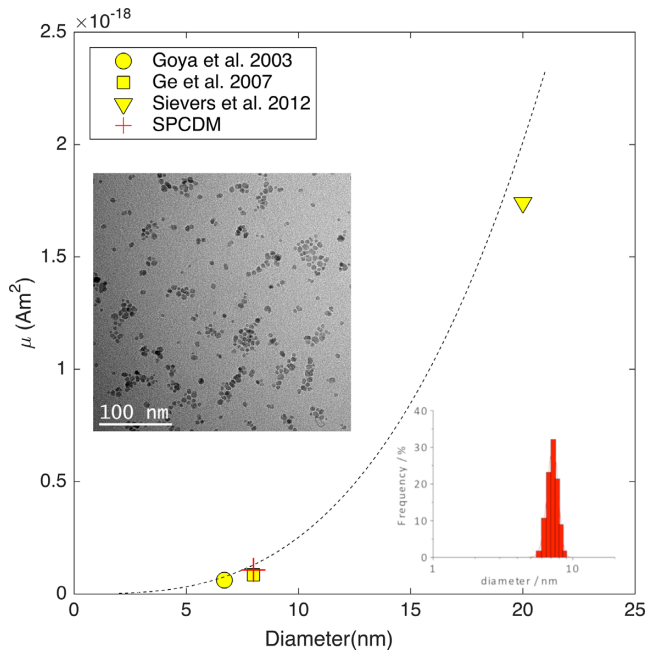
Figure 5. SPCDM estimate for the grain dipole moment (red cross) for nanoparticles of magnetite with particle size distribution diameters centred at 8(1) nm (inset histogram) and published values from previous studies. Dashed curve evaluated from constitutive equation $\mu = \sigma_S\,v$ for $\sigma_S = 480$ kAm^{-1} (saturation magnetization of magnetite). Samples with nanoparticles of magnetite and Transmission Electron Microscopy (TEM) picture (inset) provided by D.G. da Silva, S.H. Toma and K. Araki.

Figure 6. SPCDM estimates for particle concentration versus true mass concentration.

3.2 Air PM in the Jânio Quadros tunnel

Samples of air PM were collected from air quality monitoring stations in the Jânio Quadros tunnel in São Paulo, from 2004 March 23 to 25. These samples were analysed by Martins *et al.* (2006) and Sanchez-Ccoyllo *et al.* (2009) and then stored in the Laboratory of Palaeomagnetism and Rock Magnetism of IAG-USP. Each sampling day was divided into five intervals of 2 hr, from 08:00 a.m. to 18:00 p.m. The air PM samples were acquired using a Mini-Vol^{TM} Air Sampler (Airmetrics Eugene, OR, USA), with a flow volume of 7 L min^{-1} (Baldauf *et al.* 2001; Sanchez-Ccoyllo *et al.* 2009). The particulate was sieved through a sequence of 10 filters, using a MOU-DI^{TM} (micro-orifice uniform deposit impactor, MSP Corporation, Shoreview, MN, USA). As well as being analysed by the SPCDM procedure, the air PM samples were subjected to magnetic susceptibility measurements using a Multifunction Kappabridge MKF1-FA (Agico). SPCDM data were measured with a MicroMag3900-VSM (Lake Shore Cryotonics). To enhance the magnetic response, the set of 10 filtered fractions was grouped into pairs, according to adjacent grain size specifications, and then measured as a single sample.

As illustrated in Fig. 2(c), the magnetic relaxation of the air PM collected in the Jânio Quadros tunnel has a fast SP behaviour and growing IRM acquisition with increasing external fields, which is indicative of samples of mixed carriers with different properties (grain size and/or composition). A magnetic response indicating mixed contributions in air PM was also observed by Maher (2009). In the Jânio Quadros tunnel, the finer-grained minerals exhibit fast SP decay (Fig. 3b) and the coarser ones show low coercivity (1.93–4.55 mT) in the hysteresis curve; this is indicative of magnetite as a contributor in the IRM response.

SPCDM results for air PM in the Jânio Quadros tunnel are presented in Table 2. The grain dipole moment for these samples has a mean value of $1.14 \times 10^{-19} \pm 0.05$ Am^2, which does not significantly change in the time intervals in which the samples were collected. This result suggests that the magnetic properties of the air PM in the tunnel atmosphere are practically invariant, in terms of the carrier magnetic properties (size and composition) despite variable traffic conditions being observed during the test period. This result could be indicative of a uniform atmosphere in the tunnel (at least in terms of its ultrafine content properties) but it could also result from bias introduced by the filtering procedure, possibly through
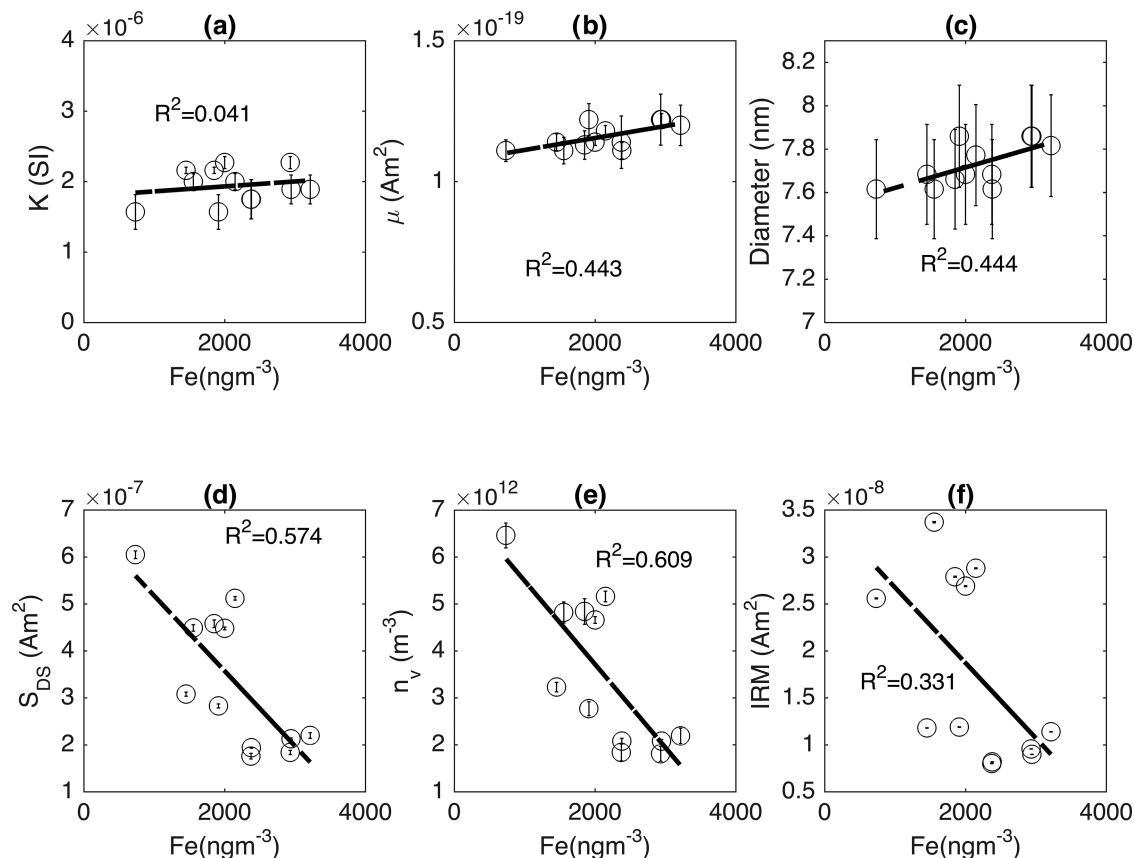
Figure 7. SPCDM results and magnetic properties for air PM collected in Jânio Quadros tunnel in São Paulo.

Table 2. SPCDM results for particulate matter in the Jânio Quadros tunnel in São Paulo, Brazil; μ and S_{DS} are the grain dipole moment and sample dipole saturation; n_v is volume-concentration of magnetic carriers (number of magnetic carrier per air flow volume in each sampling interval), and %SP the contribution of SP magnetization under external field of 1T.

Day	Sampling Interval	μ (10^{-19} Am^2)	S_{DS} (10^{-7} Am^2)	n_v (10^{12} m^{-3})	% SP
1	08:00–10:00	1.14 ± 0.09	1.76 ± 0.06	1.84 ± 0.18	98.7
	10:00–12:00	1.11 ± 0.03	1.94 ± 0.01	2.08 ± 0.06	96.5
	12:00–14:00	1.20 ± 0.07	2.20 ± 0.06	2.19 ± 0.16	95.6
	14:00–16:00	1.22 ± 0.02	2.13 ± 0.20	2.08 ± 0.03	88,9
	16:00–18:00	1.22 ± 0.05	2.83 ± 0.04	2.77 ± 0.69	96.4
2	08:00–10:00	1.11 ± 0.04	6.05 ± 0.08	6.46 ± 0.26	79.1
	10:00–12:00	1.11 ± 0.05	4.49 ± 0.07	4.82 ± 0.23	96.8
	12:00–14:00	1.18 ± 0.02	5.12 ± 0.04	5.16 ± 0.11	97.4
3	08:00–10:00	1.14 ± 0.03	3.08 ± 0.04	3.23 ± 0.10	97.5
	10:00–12:00	1.13 ± 0.05	4.58 ± 0.08	4.84 ± 0.27	98.7
	12:00–14:00	1.22 ± 0.09	1.84 ± 0.04	1.81 ± 0.16	93.5
	14:00–16:00	1.14 ± 0.01	4.48 ± 0.03	4.66 ± 0.79	97.6

selecting specific grain fractions along the chain of filters. A better evaluation is required to allow continuity of this study. The mean value of the air PM grain dipole moment is $1.14 \times 10^{-19} \pm 0.05$ Am^2, which, by applying the constitutive model $\mu = v\sigma_S$ as previously discussed, gives a mean diameter of 7.7 ± 0.1 nm for air PM in the tunnel. The estimate of such ultrafine content in the air particulate can probably be representative of a set of substances with common aerodynamic properties. From this point of view, the magnetic content in air PM may serve as a surrogate for hazardous substances (heavy metals, organics, etc.) that are also present in air PM but possibly deserving of more attention in air quality policies.

Although the magnetic carrier that comprises the air PM is rather homogeneous, its concentration covers a broad variation range. The sample dipole saturation varies from $1.76 \pm 0.06 \times 10^{-7}$ to $6.05 \pm 0.08 \times 10^{-7}$ Am^2 and corresponds to volume-concentrations from $1.84 \pm 0.18 \times 10^{12}$ to $6.46 \pm 0.26 \times 10^{12}$ m^{-3}. Despite a three-fold variation, there was no clear association with traffic density, which may suggest a dependency on sources not related to engine-combustion and contributions from sources like disk-brakes or suspended matter from pavement abrasion, among others. The %SP parameter varies from 88.9 to 98.7 per cent, suggesting that contributions from stable magnetization (in the coarser fractions) varies

from day-to-day. This result was unexpected, especially regarding the uniformity of the SP content. For all samples, the magnetization from SP contribution was prevalent.

The concentration of Fe for air PM in the Jânio Quadros tunnel (Sanchez-Ccoyllo *et al.* 2009) varies between 0.73 and 3.21 μg m^{-3} (∼4x), which is a range comparable to variations (∼3x) in sample dipole saturation ($R^2 = -0.57$, in Fig. 7d) and particle concentration ($R^2 = -0.61$ in Fig. 7e). The correlation between true Fe concentration and inverted particle concentration is an inverse one, suggesting that the SP mineral fraction decreases as Fe content increases. This kind of behaviour can be explained by assuming that the higher Fe content comprises non-ferromagnetic minerals and, therefore, has only a minor contribution to SP properties. Such incursions of high Fe content could, for example, be hosted by paramagnetic or hematite-like minerals, with secondary contributions to the SP response often being modulated by magnetite-like minerals. The possibility of a second mineral phase could also explain the minor variations in magnetic susceptibility (Fig. 7a), as all samples showed susceptibility within the error margin 2.03 ± 0.33 SI. No correlation between Fe content and the grain dipole moment (Fig. 7b) and particle diameter (Fig. 7c) can be inferred due to the uniformity of the magnetic fraction in the particulate matter of the tunnel atmosphere. The negative correlation between Fe content and IRM suggests that high iron content is not forming ferromagnetic minerals in the SD-MD fractions with stable magnetization.

4 CONCLUSION

We have presented the SPCDM procedure to enable quantitative interpretation of SP magnetization for particles with grain sizes below the characteristic diameter for stable SD grains (at least by 1 or 2 nm). This condition encompasses a wide range of fine and ultrafine particles that can be characterized using the Néel model parameters for superparamagnetism, in terms of its grain dipole moment, magnetization saturation and, from both parameters, quantitative inferences about particle concentration. A constitutive model for the grain dipole moment (in terms of grain volume and magnetization saturation) allows estimation of the grain size diameter by assuming spherical shaped particles and magnetite-like carriers. Testing by the SPCDM procedure, using synthetic samples with nanoparticles of magnetite of different concentrations, produced a clear linear dependency between inverted and true concentrations as well as correct estimates for the grain dipole moment, estimated as 7.5 ± 0.2 nm for a true distribution (TEM image) of 8.0 ± 0.7 nm. Grain dipole moment (and, therefore, grain diameter) did not vary with concentration, thus validating the proposed procedure.

For air PM samples collected in the Jânio Quadros tunnel, SPCDM provided useful information about particle diameter (7.7 ± 0.1 nm), which was well below the critical volume for stable magnetization. To our knowledge, the existence of such ultrafine particles in air PM had not previously been identified. This is a promising result, when considering better assessment of air quality related to pollutants in the fine and ultrafine fractions because magnetic particulates can serve as a surrogate for other particulate fractions exhibiting the same aerodynamic behaviour, but with deeper concerns to public health or environmental pollution. The quantitative evaluation of grain properties may also be useful in studies of provenance or proxies to evaluate assimilation of particulate pollutants by living beings. As proposed, SPCDM is well suited for ultrafine SP fractions when the equilibrium magnetization after the external field removal, is observed in a few

seconds. This procedure must be revised when handling samples with slower magnetization decay as this is indicative of coarser SP fractions. SPCDM works well however, for mixed samples with fast SP decay and stable IRM associated with low-coercivity (magnetite-like) minerals, as is characteristic of the samples analysed.

The SPCDM procedure has limitations that should be pointed out to the reader. First, since based on Langevin data fitting, the SPCDM method is well suited for SP fractions with 'fast' magnetization decay (as such, for grain-size distributions well below the thermally stable volume grains in room temperature). It is unsuited for mineral fractions with 'viscous' decays (grain volumes nearing the blocking volume) for which the relaxation times are comparable to measurement timescale. Secondly, it is assumed that the grain size of the 'fast' decay SP fraction is narrow enough (or unimodal) to be represented by a uniform grain size, as in the Néel model. Real estimates for grain size distribution may require observations with variable timescales (e.g. temperature, frequency) to reconstruct the distribution of size-dependent activation energy (Worm & Jackson 1999; Shcherbakov & Fabian 2005; Jackson *et al.* 2006; Egli 2009; Kodama 2013), which are not implemented in SPCDM. Thirdly, the magnetization saturation of the mineral SP fraction must to be known a priori to evaluate grain volume. It is not required, however, to obtain concentration estimates, which are provided by rationing two independent parameters obtained from data inversion.

REFERENCES

Aster, R.C., Borchers, B. & Thurber, C.H., 2011. *Parameter Estimation and Inverse Problems (Vol. 90),* Academic Press.

Baldauf, R.W., Lane, D.D., Marotz, G.A. & Wiener, R.W., 2001. Performance evaluation of the portable minivol particulate matter sampler, *Atmos. Environ.,* **35**(35), 6087–6091.

Bealey, W.J., McDonald, A.G., Nemitz, E., Donovan, R., Dragosits, U., Duffy, T.R. & Fowler, D., 2007. Estimating the reduction of urban PM$_{10}$ concentrations by trees within an environmental information system for planners, *J. Environ. Manage.,* **85**, 44–58.

Berkov, D.V., Görnert, P., Buske, N., Gansau, C., Mueller, J., Giersig, M., Neumann, W. & Su, D., 2000. New method for the determination of the particle magnetic moment distribution in a ferrofluid, *J. Phys. D Appl. Phys.,* **33**(4), 331.

Berndt, T., Muxworthy, A.R. & Paterson, G.A., 2015. Determining the magnetic attempt time τ_0, its temperature dependence, and the grain size distribution from magnetic viscosity measurements, *J. geophys. Res.: Solid Earth,* **120**, 7322–7336.

Byrd, R.H., Gilbert, J.C. & Nocedal, J., 2000. A trust region method based on interior point techniques for nonlinear programming, *Math. Program.,* **89**(1), 149–185.

Caldero ́n-Garciduenas, L. *et al.*, 2008. Long-term air pollution exposure is associated with neuro inflammation, an altered innate immune response, disruption of the blood-brain barrier, ultra ne particulate deposition, and

accumulation of amyloid β-42 and α-synuclein in children and young adults, *Toxicol. Pathol.,* **36**, 289–310.

Dearing, J.A., Dann, R.J.L., Hay, K., Lees, J.A., Loveland, P.J., Maher, B.A. & O'grady, K., 1996. Frequency-dependent susceptibility measurements of environmental materials, *Geophys. J. Int.,* **124**(1), 228–240.

Donaldson, K., 2003. The biological effects of coarse and fine particulate matter, *Occup Environ Med.,* **60**(5), 313–314.

Dormann, J.L. *et al.*, 1996. Thermal variation of the relaxation time of the magnetic moment of γ-Fe$_2$O$_3$ nanoparticles with interparticle interactions of various strengths, *Phys. Rev. B.,* **53**(21), 14291.

Dunlop, D.J. & Özdemir, Ö., 2001. *Rock Magnetism: Fundamentals and Frontiers (Vol. 3),* Cambridge University Press.

Egli, R., 2009. Magnetic susceptibility measurements as a function of temperature and frequency I: inversion theory, *Geophys. J. Int.,* **177**(2), 395–420.

,Evans, N., ,Baierl, A., ,Brain, P., ,Welham, SJ.and & ,Fitt, BD.(2003) Spatial Aspects of Light Leaf Spot (Pyrenopeziza brassicae) Epidemic Development on Winter Oilseed Rape (Brassica napus) in the United Kingdom. *Phytopathology* **93**, 657–65, doi:10.1094/PHYTO.2003.93.6.657, 18943051

Evans, M.E. & Heller, F., 2003. *Environmental Magnetism: Principles and Applications of Enviromagnetics,* Academic.

Fabian, K., 2003. Some additional parameters to estimate domain state from isothermal magnetization measurements, *Earth planet. Sci. Lett.,* **213**(3-4), 337–345.

Ge, J., Hu, Y., Biasini, M., Beyermann, W.P. & Yin, Y., 2007. Superparamagnetic magnetite colloidal nanocrystal clusters, *Angew. Chem. Int. Ed.,* **46**(23), 4342–4345.

Goya, G., Berquo, T., Fonseca, F. & Morales, M., 2003. Static and dynamic magnetic properties of spherical magnetite nanoparticles, *J. appl. Phys.,* **94**(5), 3520–3528.

Jackson, M., Carter-Stiglitz, B., Egli, R. & Solheid, P., 2006. Characterizing the superparamagnetic grain distribution f (V, Hk) by thermal fluctuation tomography, *J. geophys. Res.: Solid Earth,* **111**(B12) .

Jackson, M. & Solheid, P., 2010. On the quantitative analysis and evaluation of magnetic hysteresis data, *Geochem. Geophys. Geosyst.,* **11**(4).

Jasonov, P., Nourgaliev, D., Burov, B. & Heller, F., 1998. A modernized coercivity spectrometer, *Geol. Carpathica,* **49**(3), 224–226.

Jiang, Z., Liu, Q., Dekkers, M.J., Colombo, C., Yu, Y., Barrón, V. & Torrent, J., 2014. Ferro and antiferromagnetism of ultrafine-grained hematite, *Geochem. Geophys. Geosyst.,* **15**(6), 2699–2712.

Jimenez-Lopez, C., Romanek, C.S. & Bazylinski, D.A., 2010. Magnetite as a prokaryotic biomarker: a review, *J. geophys. Res.: Biogeosci.,* **115**(G2) .

Kodama, K., 2013. Application of broadband alternating current magnetic susceptibility to the characterization of magnetic nanoparticles in natural materials, *J. geophys. Res.: Solid Earth,* **118**(1), 1–12.

Li, J., Benzerara, K., Bernard, S. & Beyssac, O., 2013. The link between biomineralization and fossilization of bacteria: Insights from field and experimental studies, *Chem. Geol.,* **359**, 49–69.

Machac, T.A., Zanner, C.W. & Geiss, C.E., 2007. Time dependent irm acquisition as a tool to quantify the abundance of ultrafine superparamagnetic magnetite in loessic soils, *Geophys. J. Int.,* **169**(2), 483–489.

Maher, B.A., 2009. Rain and dust: magnetic records of climate and pollution, *Elements,* **5**(4), 229–234.

Maher, B.A. & Taylor, R.M., 1988. Formation of ultrafine-grained magnetite in soils, *Nature,* **336**(6197), 368–370.

Maher, B.A. & Thompson, R., 1991. Mineral magnetic record of the chinese loess and paleosols, *Geology,* **19**(1), 3–6.

Martins, L. *et al.*, 2006. Emission factors for gas-powered vehicles traveling through road tunnels in Sao Paulo, Brazil, *Environ. Sci. Technol.,* **40**, 6722–6729.

Maxbauer, D.P., Feinberg, J.M. & Fox, D.L., 2016. Magnetic mineral assemblages in soils and paleosols as the basis for paleoprecipitation proxies: a review of magnetic methods and challenges, *Earth Sci. Rev.,* **155**, 28–48.

Morris, W.A., Versteeg, J.K., Bryant, D.W., Legzdins, A.E., McCarry, B.E. & Marvin, C.H., 1995. Preliminary comparisons between mutagenicity and magnetic susceptibility of respirable airborne particulates, *Atmos. Environ.,* **29**, 3441–3450.

Moskowitz, B.M., Frankel, R.B. & Bazylinski, D.A., 1993. Rock magnetic criteria for the detection of biogenic magnetite, *Earth planet. Sci. Lett.,* **120**(3-4), 283–300.

Moskowitz, B.M., Frankel, R.B., Bazylinski, D.A., Jannasch, H.W. & Lovley, D.R., 1989. A comparison of magnetite particles produced anaerobically by magnetotactic and dissimilatory iron-reducing bacteria, *Geophys. Res. Lett.,* **16**(7), 665–668.

Néel, L., 1955. Some theoretical aspects of rock-magnetism, *Adv. Phys.,* **4**(14), 191–243.

Paterson, G.A., Zhao, X., Jackson, M. & Heslop, D., 2018. Measuring, processing, and analyzing hysteresis data, *Geochem. Geophys. Geosyst.,* **19**(7), 1925–1945.

Pope, C.A., III, Burnett, R.T., Thun, M.J., Calle, E.E., Krewski, D., Ito, K. & Thurston, G.D., 2002. Lung cancer, cardiopulmonary mortality, and long-term exposure to fine particulate air pollution, *JAMA,* **287**(9), 1132–1141.

Porter, S.C., 2001. Chinese loess record of monsoon climate during the last glacial–interglacial cycle, *Earth Sci. Rev.,* **54**(1-3), 115–128.

Sagnotti, L., Macri, P., Egli, R. & Mondino, M., 2006. Magnetic properties of atmospheric particulate matter from automatic air sampler stations in Latium (Italy): toward a definition of magnetic fingerprints for natural and anthropogenic PM$_{10}$ sources, *J. geophys. Res.: Solid Earth,* **111**(B12) .

Sagnotti, L. & Winkler, A., 2012. On the magnetic characterization and quantification of the superparamagnetic fraction of traffic-related urban airborne PM in Rome, Italy, *Atmos. Environ.,* **59**, 131–140.

Shcherbakov, V.P. & Fabian, K., 2005. On the determination of magnetic grain-size distributions of superparamagnetic particle ensembles using the frequency dependence of susceptibility at different temperatures, *Geophys. J. Int.,* **162**(3), 736–746.

Sievers, S., Braun, K.-F., Eberbeck, D., Gustafsson, S., Olsson, E., Schumacher, H.W. & Siegner, U., 2012. Quantitative measurement of the magnetic moment of individual magnetic nanoparticles by magnetic force microscopy, *Small,* **8**(17), 2675–2679.

Stoner, E.C. & Wohlfarth, E.P., 1948. A mechanism of magnetic hysteresis in heterogeneous alloys, *Phil. Trans. R. Soc. Lond., A,* **240**(826), 599–642.

Sánchez-Ccoyllo, O.R. *et al.*, 2009. Vehicular particulate matter emissions in road tunnels in Sao Paulo, Brazil, *Environ. Monit. Assess.,* **149**(1-4), 241–249.

Tarduno, J.A., 1995. Superparamagnetism and reduction diagenesis in pelagic sediments: enhancement or depletion? *Geophys. Res. Lett.,* **22**(11), 1337–1340.

Taylor, R., Maher, B. & Self, P., 1987. Magnetite in soils: I. the synthesis of single-domain and superparamagnetic magnetite, *Clay Miner.,* **22**(4), 411–422.

Telford, W.M., Telford, W.M., Geldart, L.P. & Sheriff, R.E., 1990. *Applied Geophysics (Vol. 1),* Cambridge University Press.

Wang, X., Løvlie, R., Zhao, X., Yang, Z., Jiang, F. & Wang, S., 2010. Quantifying ultrafine pedogenic magnetic particles in Chinese loess by monitoring viscous decay of superparamagnetism, *Geochem. Geophys. Geosyst.,* **11**(10).

Williams, W. & Muxworthy, A.R., 2006. Understanding viscous magnetization of multidomain magnetite, *J. geophys. Res.: Solid Earth,* **111**(B2).

Woodward, R.C., Heeris, J., St Pierre, T.G., Saunders, M., Gilbert, E.P., Rutnakornpituk, M., Zhang, Q. & Riffle, J.S., 2007. A comparison of methods for the measurement of the particle-size distribution of magnetic nanoparticles, *J. Appl. Crystallogr.,* **40**(s1), s495–s500.

Worm, H.U., 1998. On the superparamagnetic—stable single domain transition for magnetite, and frequency dependence of susceptibility, *Geophys. J. Int.,* **133**(1), 201–206.

Worm, H.U., 1999. Time-dependent IRM: A new technique for magnetic granulometry, *Geophys. Res. Lett.,* **26**(16), 2557–2560.

Worm, H.U. & Jackson, M., 1999. The superparamagnetism of Yucca Mountain tuff, *J. geophys. Res.: Solid Earth,* **104**(B11), 25 415–25 425.